

CLIMATE HAZARD TIMING AND FLIGHT DEMAND CO-OCCURRENCE: A DEMAND-WEIGHTED EXPOSURE FRAMEWORK

Kadek Sumaja[1,3], Tae-Ryang Tay Koo[1], Scott Mooney[2], Taha Hossein Rashidi[1]

[1] Research Centre for Integrated Transport Innovation (rCITI), School of Civil and Environmental Engineering, The University of New South Wales, Sydney
[2] School of Biological, Earth and Environmental Sciences, The University of New South Wales, Sydney
[3] Indonesian Agency for Meteorology Climatology and Geophysics

Abstract

Airport climate-risk assessments typically evaluate hazards using frequency, intensity, or projected trends, but these indicators do not capture whether hazardous conditions coincide with periods of high aviation demand. This study develops a demand-linked climate exposure framework to analyse the temporal co-occurrence between aviation climate hazards and flight activity at Sydney Airport. Daily maximum temperature, minimum temperature, precipitation, and wind variables are analysed using observational and reanalysis data for 1991–2024 and bias-corrected climate projections for 2025–2050 under SSP1–2.6 and SSP3–7.0. Hazard indicators are derived using month-specific percentile thresholds and structured into three tiers: frequency, severity, and accumulated hazard load. These metrics are combined with monthly flight activity to quantify exposed flights and flight-weighted hazard burden. The analysis focuses on exposure rather than realised disruption and excludes delay, cancellation, diversion, and vulnerability effects. Results demonstrate that aviation exposure is governed by seasonal timing rather than hazard intensity alone. A primary exposure window occurs from November to January, when heat, rainfall, and wind coincide with peak demand, with December generating the highest exposure, particularly for heat. A secondary exposure window occurs in July and is dominated by cold minimum-temperature events aligning with winter traffic. These findings demonstrate that hazard trends alone are insufficient to characterise airport climate exposure. Integrating hazard timing with aviation demand establishes a demand-weighted exposure framework for identifying operationally critical periods and supporting seasonal adaptation planning.

Keywords: Airport climate exposure, aviation demand, temporal co-occurrence, climate hazards, adaptation planning

1. Introduction

A climate hazard does not have a fixed operational impact in aviation. The same level of heat, rainfall, or crosswind can result in minimal disruption during low-demand periods but generate substantial operational impacts when it coincides with peak flight activity. For example, equivalent heat conditions may affect relatively few flights during low-demand periods but disrupt a larger proportion of operations during peak traffic, reflecting the capacity–demand balance rather than hazard intensity alone. This pattern aligns with aviation evidence demonstrating that disruption severity depends on the interaction between weather conditions and system demand, with impacts intensifying when weather-related disturbances occur under high traffic volume or constrained capacity [1], [2], [3]. Consistent with FAA guidance, weather alone does not always produce large delays; operational impacts increase when system-impacting weather coincides with excess demand or constrained capacity [4], [5]

This temporal dependence highlights a limitation in existing airport climate risk assessments, which evaluate hazards based on their physical characteristics and exposure, while overlooking how their timing interacts with system demand [4], [6]. As a result, the consequences of climate-related disruption are not proportional to hazard intensity, but are amplified under high system loading, as airports operating close to capacity experience impacts from weather-related disruptions [3], [7]. At

https://doi.org/10.71945/icas2026_0870

high traffic volumes, a delayed departure propagates through the aviation network as missed connections, extended delays, and schedule disruption, whereas similar disruption is absorbed when spare capacity is available [4], [8], [9]. Weather-related delays directly affect airport scheduling efficiency and operational performance, supporting the importance of incorporating demand conditions in assessments of climate-related aviation exposure [3]

Within the climate literature, methods exist for characterising aviation-relevant hazards. Expert Team on Climate Change Detection and Indices (ETCCDI)-based extreme indices, including extreme heat days, extreme cold nights, extreme rainfall events and percentile-based wind thresholds, provide statistically grounded approaches for measuring climate extremes [10], [11], [12]. Applied to aviation contexts, these indices demonstrate increasing extreme heat occurrence, intensifying rainfall events and growing physical stress on aviation infrastructure and operations under anthropogenic warming [13], [14], [15], [16]. However, these approaches do not account for whether hazards coincide with periods of peak flight demand, limiting their ability to represent operational risk.

The concept of co-occurrence is established in the compound-hazard literature as the simultaneous exceedance of multiple climate thresholds [12], [17], [18]. This study aims to extend that concept by examining the alignment between a climate hazard and a non-climate system variable, namely flight demand. By linking hazard timing with flight activity, this temporal co-occurrence framework captures when hazards become significant, rather than only how often or how intensely they occur.

This study examines the temporal co-occurrence between climate hazards and aviation demand to assess exposure at Sydney Airport under historical conditions and for the period 2025–2050 across SSP1–2.6 and SSP3–7.0 scenarios. The analysis focuses on exposure and does not include delay, cancellation, or operational performance data. It evaluates when climate hazards align with periods of high flight activity and therefore have operational implications. Attribution of disruption outcomes to climate hazards is not undertaken, as these outcomes are determined by multiple interacting factors, including fleet, staffing, and infrastructure conditions.

To operationalise this approach, monthly hazard indicators for aviation-relevant temperature, precipitation, and wind extremes are derived using a tiered structure of frequency, severity, and accumulated load, and integrated with observed and projected flight activity. This enables the estimation of demand-weighted exposure metrics, including affected flights and flight-weighted hazard burden, and supports systematic identification of periods in which hazard occurrence and system demand converge.

2. Data and Methods

Sydney Airport (SYD) is selected as the case study due to its role as a major national and international gateway in Australia and its exposure to temperature, precipitation, and wind hazards.

2.1. Data

Observed daily maximum temperature (tasmax), daily minimum temperature (tasmin) and precipitation (pr) for 1991–2024 were obtained from the Bureau of Meteorology national climate archives (Bureau of Meteorology, 2024). Daily wind components were derived from the BARRA2 regional atmospheric reanalysis at ~12 km resolution, providing spatial wind fields for airport-level hazard characterisation [19], [20].

Furthermore, climate projections were analysed under SSP1–2.6 and SSP3–7.0 scenarios using a six-member dynamically downscaled CMIP6 ensemble. The ensemble integrates BARPA-R and NARCliM2.0 simulations driven by ACCESS-ESM1-5, CESM2, CMCC-ESM2, EC-Earth3, MPI-ESM1-2-HR, and NorESM2-MM [19], [20], [21]. Outputs were summarised using medians and interquartile ranges to represent ensemble spread [22], [23], [24].

Scheduled flight data for Sydney Airport (August 2003–December 2025) were obtained from Cirium (retrieved April 2025). Aviation demand was defined as total flights, calculated as the sum of arrivals and departures. Flight activity for 2026–2050 was projected using ICAO post-COVID-19 scenarios, applying annual growth rates of 4.2% (central) and 3.6% (lower bound) (ICAO, 2025). Growth was applied to each calendar month using 2025 as the baseline, preserving the observed seasonal distribution.

https://doi.org/10.71945/icas2026_0870

Prior to integration, climate and flight datasets were harmonised at monthly resolution. Climate data were quality-controlled through timestamp verification, removal of implausible values, tasmin-tasmax consistency checks, and exclusion of leap days. Bias correction was calibrated over 1991-2024 and applied to historical and projected series. A hybrid Empirical Quantile Mapping-Generalised Extreme Value (EQM-GEV) approach was used for tasmax, tasmin, and pr, with EQM applied to central quantiles and GEV modelling applied to upper-tail segments [25], [26], [27], [28], [29]. Wind bias correction was applied to vector components prior to deriving wind speed and direction.

2.2. Analytical Workflow

The workflow derives monthly climate-hazard indicators and integrates them with flight activity using a two-layer exposure framework. Exposure is defined here as the co-occurrence of climate hazards and aviation activity rather than observed operational disruption. This aligns with the IPCC Sixth Assessment Report, which concludes that hot extremes will increase, cold extremes will decrease, and heavy precipitation will intensify with global warming [30].

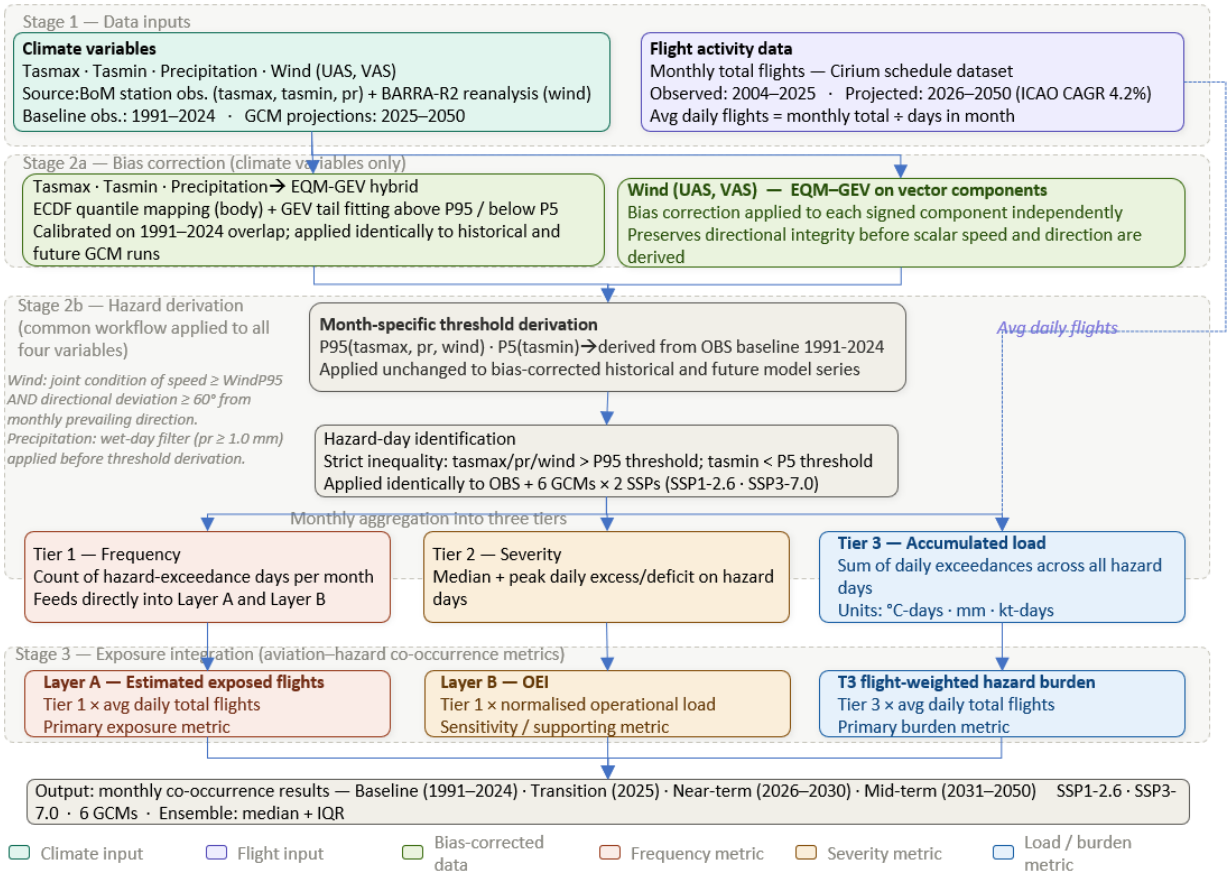


Figure 1. The hazard–demand co-occurrence framework. The framework links climate hazard derivation, tiered aggregation, and exposure metrics with flight activity data. It highlights how temporal alignment between hazards and demand is operationalised to identify aviation exposure hotspots.

All hazards are defined using a threshold-based approach. Month-specific percentiles are derived from the 1991–2024 baseline. Daily observations are grouped by calendar month, and leap days are removed. Upper-tail hazards use the 95th percentile, while minimum-temperature deficits use the 5th percentile. Specifically, TX95p, TN5p, R95p, and Wind95p represent the monthly percentiles of tasmax, tasmin, wet-day precipitation, and wind speed, respectively. Hazard exceedance is defined using strict inequality, consistent with Expert Team on Climate Change Detection and Indices (ETCCDI) conventions [10], [31]. These thresholds are applied to both observations and bias-corrected projections, ensuring comparability across hazards, scenarios, and periods and avoiding redefinition of extremes under warming conditions [12], [32], [33].

Following this, daily hazard series are aggregated into monthly indicators using a three-tier structure:

https://doi.org/10.71945/icas2026_0870

Tier 1 quantifies hazard-day frequency, Tier 2 summarises daily excess or deficit magnitudes, and Tier 3 represents accumulated monthly hazard load. This structure reflects the combined influence of frequency and magnitude on operational stress [34], [35], [36], [37]. These monthly indicators are then integrated with flight activity to quantify aviation exposure. Three metrics are derived: Layer A estimates the number of flights occurring on hazard days, Layer B scales hazard frequency by relative operational load, and Tier 3 flight-weighted burden combines accumulated hazard load with traffic volume.

Layer A (Estimated Flights Exposed) quantifies the number of flights occurring on hazard-exceedance days as the product of monthly hazard frequency and average daily total flights. These metric expresses exposure as estimated flights per month.

$$LayerA = \text{Hazard Frequency} * Avg\ Daily\ Total\ Flights \quad (1)$$

Where hazard frequency is expressed in days per month and average daily total flights in flights per day. Layer A therefore relates hazard occurrence directly to aviation activity.

Layer B, or Operational Exposure Intensity, scales hazard frequency by operating load, defined as the ratio of monthly average daily flights to the 2004–2025 baseline mean. The COVID-19 years were retained in this baseline normalisation, meaning that Layer B is anchored to the observed traffic record rather than to a pre-pandemic-only reference period. This metric indicates whether hazard days occur during months of above-average traffic relative to the operating history.

$$\text{Normalised Operational Load}_{y,m} = \frac{\text{Avg Daily Total Flights}_{y,m}}{\overline{\text{Avg Daily Total Flights}}_{2004-2024}} \quad (2)$$

$$\text{Layer B}_{y,m} = \text{Hazard Frequency}_{y,m} \times \text{Normalised Operational Load}_{y,m} \quad (3)$$

Where y denotes year and m denotes calendar month, the numerator corresponds to the average daily flights for a given year–month, while the denominator is defined as the mean of monthly average daily flights over the 2004–2024 baseline period. This two-stage averaging expresses daily flight counts as monthly average daily values and then normalises them relative to the baseline operating level. Values greater than 1 indicate above-baseline traffic, while values below 1 indicate below-baseline traffic.

Finally, tier 3 flight-weighted hazard burden multiplies accumulated monthly hazard load by average daily flights, quantifying the interaction between cumulative hazard intensity and traffic volume:

$$\text{T3 Flight-Weighted Burden}_{y,m} = \text{Tier 3 Accumulated Hazard Load}_{y,m} \times \text{Avg Daily Total Flights}_{y,m} \quad (4)$$

In equation 4, accumulated hazard load refers to the sum of daily exceedance magnitudes within a year–month. For heat, it is the sum of daily temperature exceedance above the TX95p threshold across all hazard days; for cold, it is the sum of daily temperature deficit below the TN5p threshold; for rainfall and wind, it is the summed exceedance above the R95p or WindP95 threshold. Unlike Tier 1 frequency, which counts hazard days, accumulated hazard load captures both the number of hazard days and how far each event exceeds the threshold. The Tier 3 flight-weighted burden identifies months in which accumulated hazard intensity coincides with high operational demand.

The workflow is applied consistently across all hazards, scenarios, and analysis periods. Ensemble outputs are summarised using medians and interquartile ranges for the baseline (1991–2024), transition year (2025), near-term period (2026–2030), and mid-term period (2031–2050) [22], [24].

2.3. Hazard-Specific Variable Definitions and Index Construction

The workflow was applied to four hazard variables: maximum temperature, minimum temperature, precipitation and wind. Table 1 summarises the hazard components, including the input variable, data source, threshold index, hazard-day condition and Tier 2 extreme indicator.

 https://doi.org/10.71945/icas2026_0870

Table 1. Hazard-specific variable definitions applied within the analytical workflow.

Hazard	Input variable	Source	Primary index	Hazard-day condition	Tier 2 extreme (Median/mean/peak)
Extreme heat	Daily maximum temperature (tasmax, °C)	BoM observations and CMIP6 ensemble model derived from BARPA-R	TX95p (95th percentile of daily tasmax per calendar month)	tasmax > monthly TX95p	exceedance above TX95p threshold (°C)
Cold minimum temperature	Daily minimum temperature (tasmin, °C)	BoM observations and CMIP6 ensemble model derived from BARPA-R	TN5p (5th percentile of daily tasmin per calendar month)	tasmin < monthly TN5p	deficit below TN5p threshold (°C)
Heavy rainfall	Daily precipitation (pr, mm)	BoM observations and CMIP6 ensemble model derived from BARPA-R	R95p (95th percentile of wet-day precipitation per calendar month)	pr > monthly R95p	rainfall excess above R95p threshold (mm)
Directional high wind	Daily wind speed (knots) and direction (°), derived from UAS and VAS components	BARRA-R2 reanalysis and CMIP6 ensemble model derived from BARPA-R	Wind95p (95th percentile of daily wind speed per calendar month)	speed ≥ Wind95p AND directional deviation ≥ 60°	wind-speed excess above Wind95p threshold under directionally unfavourable conditions (kt)

Precipitation and wind thresholds differ from temperature-based indices and therefore require additional specification. For precipitation, R95p thresholds are derived from wet-day observations, defined as daily precipitation ≥ 1.0 mm, in accordance with ETCCDI conventions (Zhang et al., 2011; Seneviratne et al., 2021). This excludes trace rainfall and ensures that thresholds reflect rainfall events relevant to operational conditions. Monthly Tier 3 precipitation load represents the cumulative exceedance above R95p across all hazard days, expressed in millimetres.

Wind variables are derived from eastward (UAS) and northward (VAS) components from the BARRA-R2 reanalysis, which provides spatially coherent wind fields in locations where direct observations are limited (Bureau of Meteorology, 2023; Su et al., 2022). Wind speed is calculated as $\sqrt{}$ (UAS² + VAS²) and converted to knots, while wind direction is expressed clockwise from north. Monthly prevailing wind direction is estimated using circular statistics applied to non-calm baseline days (wind speed ≥ 1 kt). A wind hazard day is defined when wind speed exceeds the monthly Wind95p threshold and directional deviation from the prevailing direction is at least 60°. Monthly Tier 3 wind load represents the cumulative wind-speed exceedance above Wind95p across all hazard days, expressed in knot-days.

3. Result and Finding

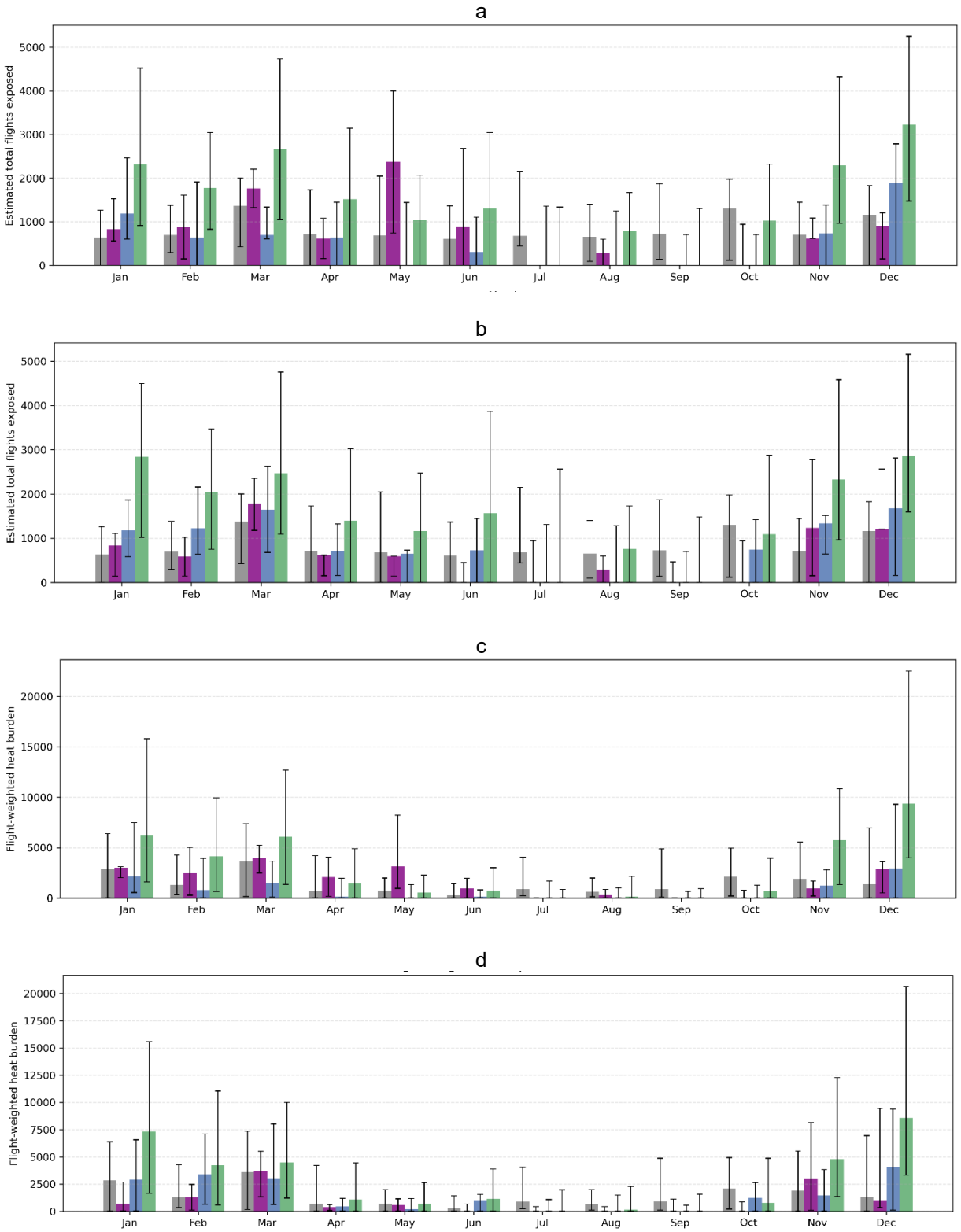
The results show that aviation exposure at Sydney Airport is concentrated in two monthly windows. The main window is November–January, where heat and wind exposure coincide with projected traffic demand and rainfall adds an episodic November–December burden; December produces the multi-hazard and flight-weighted signal. A July window is driven by residual cold-event exposure. These patterns arise from linking monthly hazard occurrence with flight activity and would be obscured in period-level or hazard-only summaries. The following sections examine each hazard to identify its

https://doi.org/10.71945/icas2026_0870

monthly exposure patterns and associated burden mechanisms and integrate these results in a cross-hazard synthesis to identify the dominant operational exposure windows.

3.1 Extreme Heat (Tasmax)-Related Flight Exposure and Flight-Weighted Heat Burden

Figure 2 summarises extreme-heat exposure metrics. Layer A estimates the number of flights coinciding with TX95p exceedance days, while Tier 3 flight-weighted heat burden integrates accumulated heat load with flight activity. These metrics distinguish months where exposure is driven by the number of affected flights from those where high exposure coincides with cumulative heat burden.



https://doi.org/10.71945/icas2026_0870

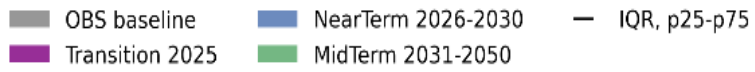


Figure 2 – Extreme-heat aviation exposure and flight-weighted heat burden at Sydney Airport: (a) Layer A exposure (SSP1–2.6); (b) Layer A exposure (SSP3–7.0); (c) T3 flight-weighted heat burden (SSP1–2.6); (d) T3 flight-weighted heat burden (SSP3–7.0).

Extreme heat demonstrates concurrent increases in hazard frequency, accumulated heat load, and projected flight activity, producing the strongest co-occurrence signal in December. Under mid-term conditions (2031–2050), December emerges as the principal exposure month, as extreme heat days, Tier 3 accumulated heat load and peak traffic volumes coincide. Heat frequency increases from 2.0 to 3.0 days, while Tier 2 severity rises from 2.25°C above the threshold to 3.09°C under SSP1–2.6 and 2.80°C under SSP3–7.0. Tier 3 accumulated heat load increases more strongly, from 2.10°C-days to 9.17 and 7.45°C-days. When combined with projected traffic growth, Layer A increases from 1,158 to 3,226 and 2,860 exposed flights, while Tier 3 flight-weighted heat burden rises from 1,342 to 9,361 and 8,551.

January constitutes a secondary exposure month characterised by a different mechanism. Layer A increases from 640 to 2,318 and 2,846 exposed flights, while Tier 2 severity declines from 5.07°C to approximately 3.1°C under both scenarios. This pattern indicates that January exposure is driven primarily by alignment between hazard occurrence and traffic volume rather than intensification of individual heat events. March and November exhibit similar patterns, with increasing exposure despite declining severity. December differs in that hazard intensification and traffic growth reinforce each other, whereas other months are driven predominantly by increasing demand.

Figure 3 clarifies the difference between hazard occurrence and aviation exposure for extreme heat. Although TX95p hazard-day frequency increases in several months under SSP3–7.0 mid-term conditions, the Layer A response is amplified where these hazard days coincide with higher flight activity. This comparison helps explain why December and January show large exposure increases.

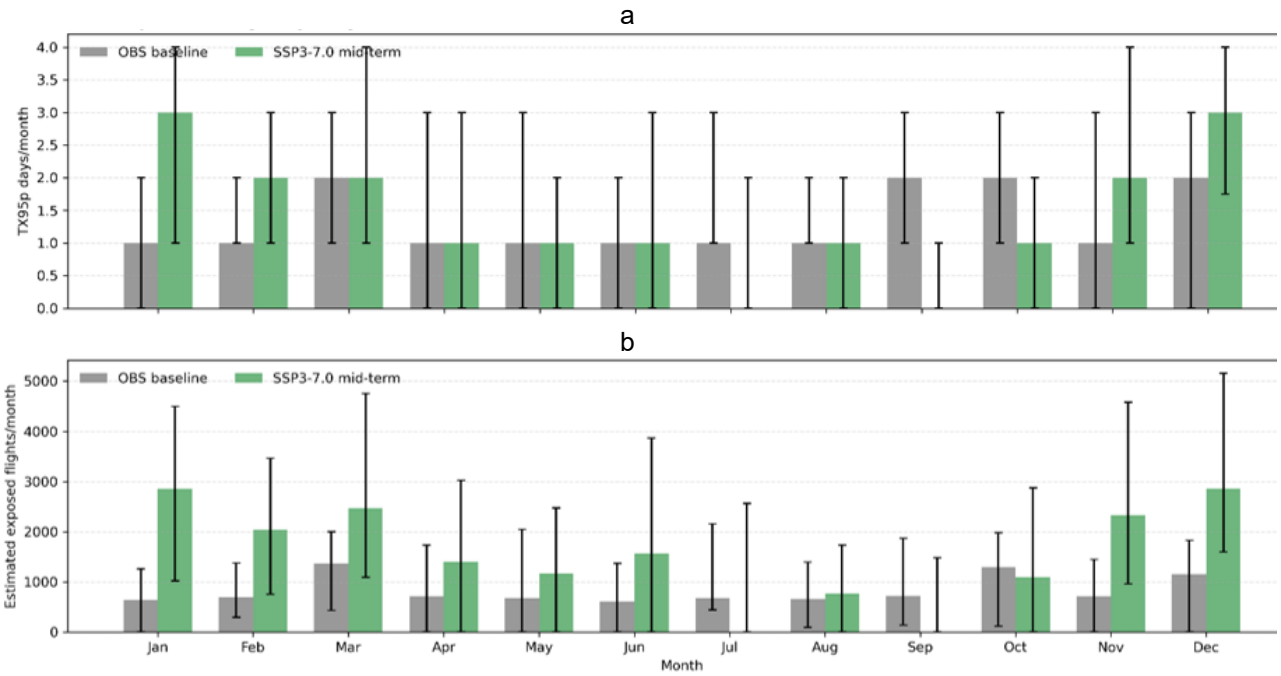


Figure 3 – Monthly (a) TX95p hazard frequency and (b) Layer A aviation exposure under baseline and SSP3–7.0 mid-term conditions.

As shown in Figure 2, changes in hazard frequency alone do not fully account for the observed exposure pattern. Several months show modest increases in TX95p frequency, whereas Layer A exposure rises more strongly when hazard days align with periods of higher traffic demand. This is evident in December and January, confirming that projected aviation exposure reflects both hazard occurrence and the seasonal distribution of flight activity.

Overall, the results demonstrate that December represents the most robust and policy-relevant

https://doi.org/10.71945/icas2026_0870

period, as hazard intensification and traffic growth reinforce one another. In contrast, January and other months are characterised predominantly by traffic-driven exposure, with limited contribution from increasing hazard intensity.

3.2 Cold Minimum Temperature (Tasmin) exposure

By comparison, cold minimum temperature exposure exhibits the opposite behaviour. While the overall cold-hazard signal declines under warming, a persistent July exposure window remains. Under SSP3–7.0 mid-term conditions, median TN5p frequency, Layer A exposure and Tier 3 cold burden reduce to zero in aggregated results, while SSP1–2.6 retains only a weak residual signal. However, these aggregate statistics obscure consistent July exposure across all periods and scenarios, with approximately 1,500–3,100 exposed flights and Tier 3 burden exceeding 1,100.

This July persistence is not associated with increasing cold severity. Instead, the July deficit declines from 1.55°C to 0.61°C under SSP1–2.6, indicating weakening cold extremes. The remaining exposure is therefore explained by the temporal alignment between residual cold events and winter flight demand rather than hazard amplification. Cold exposure persists at the monthly scale despite declining hazard intensity, reflecting demand-driven co-occurrence rather than climatic strengthening.

3.3 Heavy rainfall (precipitation) exposure and flight activity

Heavy rainfall demonstrates an event-driven exposure pattern. Period-level medians for R95p exceedance days, Layer A exposure, and flight-weighted burden are zero in the baseline and remain zero under mid-term scenarios, indicating that rainfall exposure is concentrated in extreme events rather than distributed across typical months. This is evident in the divergence between medians and means: under SSP3–7.0 mid-term conditions, December mean accumulated rainfall load reaches 27.70 mm compared with a median of 3.86 mm, while mean flight-weighted burden reaches 31,813 mm-flights compared with 4,718 mm-flights. These differences confirm that rainfall exposure is dominated by tail events.

Within this episodic structure, November and December are the principal exposure months, as R95p events coincide with elevated flight activity. Under SSP1–2.6 near-term conditions, median Layer A exposure reaches 685 and 668 flights, increasing to 858 and 873 flights under SSP3–7.0 mid-term conditions. Mean December exposure under SSP3–7.0 rises to 1,375 flights compared with 312 flights in the baseline. Rainfall exposure therefore operates as a peak-event mechanism concentrated in late spring and early summer. This timing overlaps with the primary heat-exposure window, forming a compound seasonal exposure period even in the absence of same-day co-occurrence. Therefore, during this interval, extreme rainfall events and elevated heat exposure can affect a high number of flights within the same seasonal window, even when the hazards do not occur concurrently on individual days.

3.4 High Wind Related Flight Exposure

Wind demonstrates a contrasting pattern characterised by traffic-amplified exposure. Median Wind95p frequency remains zero across the baseline and mid-term scenarios, while mean frequency changes only marginally from 0.90 to approximately 0.93–0.96 days per month. This indicates limited change in wind occurrence. Exposure increases because these events coincide with higher projected flight volumes, indicating that wind-related burden is driven primarily by traffic growth rather than changes in hazard intensity.

Wind exposure is concentrated in high-traffic months. April to September record zero median Layer A exposure, while January, October, and December emerge as the principal exposure periods. Under SSP1–2.6 mid-term conditions, January reaches 2,019 exposed flights, followed by October (1,812) and December (1,517). Under SSP3–7.0, January increases to 2,325, followed by October (1,750) and December (1,613). Tier 3 flight-weighted burden follows the same pattern, with January reaching approximately 3,400 kt-flights compared with a baseline October peak of approximately 1,984 kt-flights. This shift reflects increasing traffic volumes rather than stronger wind events.

Wind therefore differs from heat and rainfall in that its exposure signal is dominated by demand growth rather than hazard intensification. Although it overlaps with the broader November–January high-traffic period, the projected burden reflects a greater number of flights encountering largely stable wind conditions. Wind contributes to seasonal exposure pressure through traffic amplification

https://doi.org/10.71945/icas2026_0870

rather than changes in the physical hazard regime.

3.5 Cross-Hazard Synthesis

Hazard-specific results demonstrate that aviation exposure is determined not by hazard frequency alone but by the timing of hazard occurrence relative to seasonal flight demand. This section synthesises patterns across all four hazards to identify the months in which exposure is elevated, to distinguish hazard-driven from traffic-amplified co-occurrence, and to assess whether high-exposure periods correspond to elevated accumulated hazard burden.

Cross-hazard patterns are identified using Layer A exposure (Table 2) and Tier 3 flight-weighted burden (Table 3). Table 2 identifies months with non-zero median exposure across multiple hazards or persistent single-hazard signals, while Table 3 evaluates whether these periods also exhibit elevated accumulated hazard load.

Table 2. Mid-term Layer A cross-hazard exposure for Sydney Airport, 2031–2050**.**

Month	TASMAX SSP370 [IQR]	TASMAX SSP126	TASMIN SSP370 [IQR]	TASMIN SSP126	PR SSP370 [IQR]	PR SSP126	WIND SSP370 [IQR]	WIND SSP126
Jan	**2,846 [1,020–4,495]**	**2,318**	0 [0–1,485]	0	0 [0–1,279]	0	**2,325 [949–3,429]**	**2,019**
Feb	2,047 [753–3,464]	1,777	0 [0–1,043]	0	0 [0–754]	0	1,020 [0–1,769]	1,284
Mar	2,466 [1,090–4,755]	2,678	0 [0–973]	0	0 [0–973]	0	869 [0–1,759]	784
Apr	1,398 [0–3,021]	1,517	0 [0–0]	0	0 [0–0]	0	0 [0–0]	0
May	1,168 [0–2,472]	1,032	0 [0–1,582]	0	0 [0–0]	0	0 [0–0]	0
Jun	1,564 [0–3,869]	1,300	1,173 [0–3,077]	1,658	0 [0–0]	0	0 [0–0]	0
Jul	0 [0–2,561]	0	**1,982 [0–3,726]**	**2,527**	0 [0–0]	0	0 [0–0]	0
Aug	765 [0–1,730]	781	1,228 [0–2,954]	1,594	0 [0–0]	0	0 [0–0]	0
Sep	0 [0–1,478]	0	1,280 [0–2,821]	1,449	0 [0–0]	0	0 [0–1,064]	0
Oct	1,091 [0–2,875]	1,025	1,005 [0–2,508]	1,750	0 [0–1,221]	0	**1,750 [897–3,210]**	**1,812**
Nov	**2,330 [961–4,578]**	**2,289**	0 [0–1,719]	0	**858 [0–1,657]**	**395**	**1,581 [824–2,687]**	**1,322**
Dec	**2,860 [1,594–5,157]**	**3,226**	0 [0–1,678]	0	**873 [0–2,080]**	**855**	**1,613 [796–2,769]**	**1,517**

Note: Values represent ensemble median exposed flights per month. SSP3–7.0 results are reported with interquartile ranges (p25–p75), while SSP1–2.6 medians are included for comparison. Zero medians indicate no hazard-day co-occurrence in the typical modelled month; non-zero upper IQR values indicate intermittent exposure. Bold values identify cross-hazard priority months.

Table 3. Mid-term Tier 3 flight-weighted hazard burden for selected hazard–month combinations.

Hazard–Month	Baseline	Mid-term SSP1–2.6 (%Δ)	Mid-term SSP3–7.0 (%Δ)
TASMAX Dec	1,342.1	9,360.6 (+597.5%)	8,551.0 (+537.1%)
TASMAX Nov	1,880.8	5,754.0 (+205.9%)	4,778.7 (+154.1%)

https://doi.org/10.71945/icas2026_0870

TASMAX Jan	2,852.1	6,181.3 (+116.7%)	7,318.4 (+156.6%)
TASMIN Jul	0.0	1,625.4 (n.a.)	1,155.2 (n.a.)
TASMIN Jun	132.1	1,174.1 (+788.7%)	563.1 (+326.2%)
PR Dec	0.0	2,379.5 (n.a.)	4,718.5 (n.a.)
PR Nov	0.0	766.1 (n.a.)	1,299.5 (n.a.)
WIND Jan	317.7	3,456.2 (+987.8%)	3,342.8 (+952.1%)
WIND Nov	523.1	1,710.7 (+227.1%)	1,964.2 (+275.5%)
WIND Dec	479.4	2,261.9 (+371.8%)	2,682.8 (+459.6%)
WIND Oct	1,983.8	2,611.0 (+31.6%)	2,439.4 (+23.0%)

Note: Values represent ensemble medians. Percentage change is calculated relative to the observed baseline median. Not applicable indicates that percentage change was not calculated because the baseline median is zero; absolute mid-term burden is reported instead. TASMAX and TASMIN are reported as flight-weighted thermal burden, PR as mm-flight, and WIND as kt-flight. Precipitation and wind Tier 3 burdens exhibit right-skewed distributions, with most months showing low or zero burden and a small number of months exhibiting substantially higher values. Median values are reported for consistency, while illustrative mean values are discussed in the text to capture the influence of tail events.

Table 2 presents mid-term Layer A exposure across all months and hazards under SSP1–2.6 and SSP3–7.0. Zero medians indicate no hazard-day co-occurrence, whereas non-zero upper interquartile ranges indicate intermittent exposure. Table 3 reports Tier 3 burden for priority hazard–month combinations, providing an intensity-weighted measure of exposure. There are three cross-hazard patterns emerge from Tables 2 and 3.

Pattern 1 indicates multi-hazard exposure occurs between November and January. These months show overlapping heat and wind exposure, with rainfall contributing in November and December. December records non-zero median Layer A exposure for TASMAX, precipitation, and wind, representing the only month with three hazards co-occurring at the monthly median scale. Tier 3 results confirm elevated accumulated burden across hazards, with heat, wind, and rainfall all contributing to increased exposure. This pattern reflects seasonal co-occurrence of hazards with high flight demand rather than same-day concurrence.

Pattern 2 identifies a winter cold-exposure window occurs in July. This period is dominated by TASMIN and shows no multi-hazard overlap at the monthly median level. Both Layer A and Tier 3 values remain non-zero, indicating persistent alignment between cold events and winter traffic demand. The near-stable amplification ratio indicates persistence rather than growth, and this signal is only resolved when hazard indicators are linked to monthly demand rather than aggregated at longer timescales.

Pattern 3 demonstrates that traffic demand is a primary driver of exposure magnitude. Exposure increases where hazard occurrence coincides with higher flight volumes. This is most evident for wind, where frequency changes little but both Layer A and Tier 3 burden increase across high-demand months. A similar mechanism applies to rainfall, where episodic events generate high burden when coinciding with peak traffic. Hazard-only analysis does not capture this amplification effect.

https://doi.org/10.71945/icas2026_0870

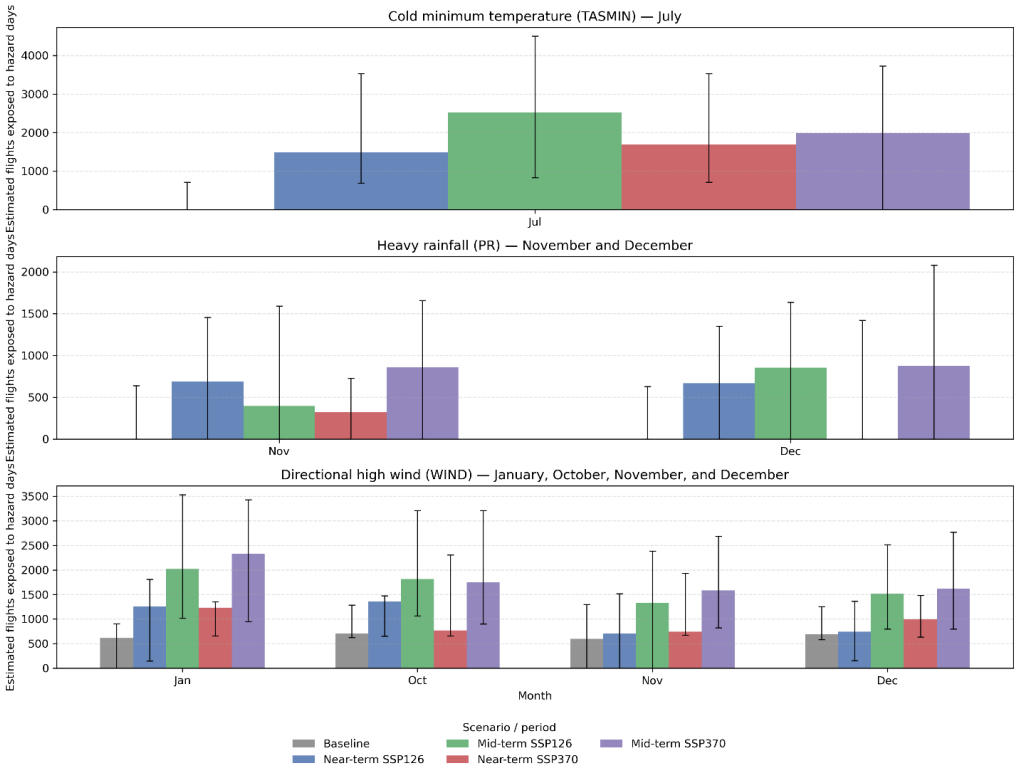


Figure 4 – Selected non-heat exposure windows across cold minimum temperature, heavy rainfall, and directional high wind

Figure 4 illustrates these mechanisms for non-heat hazards. It shows persistent winter cold exposure, episodic rainfall exposure in late spring and early summer, and traffic-amplified wind exposure during high-demand months. Differences in axis scale reflect variation in exposure magnitude across hazards.

4. Discussion

4.1 Climate-Related Aviation Exposure Is a Timing Problem

Papers are accepted on the basis that they may be

Results across all four hazards indicate that aviation exposure at Sydney Airport is temporally concentrated. The question is whether heat, cold, rainfall, or wind intensify under warming, and when hazard days coincide with periods of high flight demand. This distinction is captured by the tiered hazard–flight co-occurrence framework and extends hazard-trend analyses by linking monthly hazard indicators with projected aviation activity [14], [15].

This interpretation is consistent with the IPCC risk framing, in which risk arises from the interaction of hazard, exposure, and vulnerability [30]. Although vulnerability factors, including aircraft performance constraints, runway configuration, staffing, and recovery capacity, are not quantified, exposure is operationalised through the temporal alignment between monthly hazard indicators and flight activity. The framework therefore does not predict realised disruption; instead, it identifies hazard–exposure convergence at operationally relevant timescales [30]

Exposure is concentrated in two seasonal windows. The primary window spans November to January, when heat, rainfall, and wind coincide with projected flight volumes. December stands out, with non-zero median Layer A exposure across all three hazards and the highest Tier 3 heat burden among the hazard–month combinations. This pattern cannot be explained by hazard intensification alone. Heat exposure is driven by increases in both frequency and accumulated burden (figure 2)., whereas rainfall and wind exposure are shaped by event timing and alignment with traffic demand.

By contrast, the secondary window occurs in July and is dominated by cold minimum temperature. Across scenarios and projection periods, July shows persistent cold-related co-occurrence without multi-hazard overlap at the monthly median level. This indicates that residual cold events align with winter flight demand rather than reflecting intensifying cold conditions (need support citation). The stability of this pattern from near-term to mid-

https://doi.org/10.71945/icas2026_0870

term projections suggests persistence (need evidence), and the signal becomes clearer when hazard indicators are analysed in relation to demand rather than aggregated at the period level.

These findings show that aviation exposure at Sydney Airport is structured by seasonal timing. The November - January window represents multi-hazard exposure during high-demand months, whereas July captures a distinct cold-specific exposure window. This distinction is critical for interpretation: similar hazard frequencies can have different operational implications depending on when they occur relative to aviation demand.

4.2 Hazard mechanisms and operational implications differ

The four hazards show exposure mechanisms, implying different planning priorities. Heat is the case of combined physical and demand-driven amplification. In December, heat frequency, severity, accumulated load, and projected flight volumes increase, producing the highest co-occurrence burden in the analysis. This is relevant because high temperatures can reduce air density, lift, and take-off performance, potentially leading to payload restrictions or longer take-off requirements [13], [38]. Heat-related impacts extend to ground operations, worker safety, pavement performance, and infrastructure resilience [14], [15], [39]. January shows a different mechanism: exposure increases while severity declines, indicating that co-occurrence can also arise from the timing of hazard days relative to traffic demand rather than from intensifying heat alone.

In contrast, wind exposure increases through traffic amplification. Wind frequency remains stable, but exposure rises when wind events coincide with higher projected flight volumes. This matters because crosswinds, tailwinds, and wind shifts affect runway configuration, landing and take-off conditions, airport capacity, and schedule reliability [6], [40]. The planning implication is less about structural escalation of wind hazard and more about maintaining runway flexibility, scheduling resilience, and contingency capacity during high-demand months [39], [41].

Rainfall follows an event-driven pattern, with exposure concentrated in November and December when rainfall events align with peak traffic. This points to preparedness for disruption rather than continuous pressure. Extreme precipitation has been linked to flood-management challenges, drainage constraints, airport waterlogging, and operational disruption, supporting the relevance of drainage capacity, surface-water management, and contingency planning during high-exposure periods [42], [43], [44], [45].

Cold minimum temperature shows the opposite pattern. Although the cold signal declines under warming, a July exposure window persists because cold events continue to align with winter flight demand. Declining severity indicates that this persistence is driven by timing rather than hazard intensification. Cold-related planning concerns maintaining seasonal readiness for winter events, including de-icing, snow and ice control, and winter-operation preparedness, rather than responding to a growing cold-hazard signal [5], [46], [47].

4.3 Hazard mechanisms and operational implications differ

The contribution of this study is methodological and practical. Methodologically, this study demonstrates that airport climate exposure cannot be assessed from hazard trends alone. Hazard-based approaches, including ETCCDI-style percentile indices, threshold exceedances, and return-period analyses, quantify the frequency and intensity of climate extremes but do not capture whether these events coincide with periods of high aviation demand [10], [30], [31]. To address this limitation, monthly hazard indicators are linked with observed and projected flight activity, allowing exposure to be quantified as estimated exposed flights and flight-weighted hazard burden. The framework advances co-occurrence analysis by integrating climate variables with an operational factor, aviation demand, and operationalises the frequency–intensity–load structure of climate extremes within a demand-weighted exposure framework consistent with the IPCC risk model [10], [17], [18], [30].

Practically, the framework produces a calendar of operational exposure for Sydney Airport. It identifies December as the exposure month, November–January as the late-spring-to-summer exposure window, and July as a winter exposure window obscured in period-level statistics. These findings are relevant to airport operators, airlines, ground handlers and aviation climate-risk planners because they indicate when heat-readiness, drainage preparedness, wind-related operational flexibility, schedule buffers, workforce planning and cold-event contingency measures are needed

 https://doi.org/10.71945/icas2026_0870

[1], [2], [3], [16]. The framework does not predict disruption; it identifies when hazard conditions and traffic demand combine to create exposure potential.
Applying this framework, the study identifies December as the principal aviation-climate exposure month, indicates that hazards produce exposure through distinct adaptation strategies, and demonstrates that period-level summaries can obscure monthly exposure patterns.

4.4 Hazard mechanisms and operational implications differ

The interpretation of results is constrained by several limitations. Exposure is defined as temporal alignment rather than observed disruption, and cross-hazard synthesis does not assess same-day concurrence. Monthly aggregation smooths intra-day and intra-week variability. Traffic projections rely on a deterministic growth assumption, thereby underrepresenting demand uncertainty, while hazard thresholds remain fixed to historical conditions and do not account for adaptive changes in operational tolerance.

Within these constraints, the analysis demonstrates that aviation climate risk at Sydney Airport is primarily governed by timing rather than hazard magnitude alone. While heat intensification is evident, its operational impact is concentrated in December, where hazard occurrence aligns with peak demand. Rainfall contributes to this late spring to summer exposure through episodic high-burden events, while wind increases exposure through alignment with high traffic volumes. In contrast, cold conditions, despite an overall decline, retain a distinct July exposure window that is not captured in aggregated analyses.

Overall. climate risk cannot be derived from hazard trends alone. The critical factor is the temporal alignment between hazard occurrence and operational demand. This alignment defines concentrated exposure windows and hazard-specific mechanisms, indicating the need for focused, timing-dependent adaptation strategies.

Contact Author Email Address
k.sumaja@unsw.edu.au

Copyright Statement
The authors confirm that they, and/or their affiliated institution or organisation, hold the copyright for all original material in this paper. The authors confirm that permission has been obtained from copyright holders for any third-party material included. The authors grant permission for this paper to be published and distributed as part of the ICAS proceedings, including individual off-prints, in accordance with ICAS publication policies.

Acknowledgements
This paper is supported by the Indonesian Endowment Fund for Education (LPDP) scholarship.

References

[1] C.-L. Wu and K. Law, ‘Modelling the delay propagation effects of multiple resource connections in an airline network using a Bayesian network model’, *Transp. Res. E Logist. Transp. Rev.*, vol. 122, pp. 62–77, Feb. 2019, doi: 10.1016/j.tre.2018.11.004.
[2] Y. Wang, M. Z. Li, K. Gopalakrishnan, and T. Liu, ‘Timescales of delay propagation in airport networks’, *Transp. Res. E Logist. Transp. Rev.*, vol. 161, p. 102687, May 2022, doi: 10.1016/j.tre.2022.102687.
[3] Á. Rodríguez-Sanz, J. Cano, and B. Rubio Fernández, ‘Impact of Weather Conditions on Airport Arrival Delay and Throughput’, *Aircraft Engineering and Aerospace Technology*, vol. 94, no. 1, pp. 60–78, Jan. 2022, doi: 10.1108/AEAT-12-2020-0318.
[4] Federal Aviation Administration, ‘Traffic Management Overview.’, Traffic Management Overview. Accessed: May 16, 2026. [Online]. Available: https://www.faa.gov/nextgen/programs/weather/tfm_support/overview
[5] Federal Aviation Administration, ‘What is the largest cause of delay in the National Airspace System?’,

FAQ: Weather Delay. Accessed: May 16, 2026. [Online]. Available: https://www.faa.gov/nextgen/programs/weather/faq
[6] ICAO, '2022 Environmental Report', Montreal, Canada, 2022. Accessed: Nov. 04, 2024. [Online]. Available: https://www.icao.int/environmental-protection/Documents/EnvironmentalReports/2022/ICAO%20ENV%20Report%202022%20F4.pdf
[7] M. Schultz, S. Lorenz, R. Schmitz, and L. Delgado, 'Weather Impact on Airport Performance', 2018. doi: 10.3390/aerospace5040109.
[8] M. Janic, 'Light rail rapid transit systems for more sustainable ground accessibility of airports', *Transportation Planning and Technology*, vol. 34, no. 6, pp. 569–592, 2011, doi: 10.1080/03081060.2011.600073.
[9] V. K. Chauhan *et al.*, 'Network science approach for identifying disruptive elements of an airline', *Data Science and Management*, vol. 6, no. 2, pp. 110–121, Jun. 2023, doi: 10.1016/j.dsm.2023.04.001.
[10] X. Zhang *et al.*, 'Indices for monitoring changes in extremes based on daily temperature and precipitation data', *WIREs Climate Change*, vol. 2, no. 6, pp. 851–870, Nov. 2011, doi: 10.1002/wcc.147.
[11] A. L. Hirsch *et al.*, 'Amplification of Australian Heatwaves via Local Land-Atmosphere Coupling', *Journal of Geophysical Research: Atmospheres*, vol. 124, no. 24, pp. 13625–13647, Dec. 2019, doi: 10.1029/2019JD030665.
[12] M. M. Vogel, J. Zscheischler, E. M. Fischer, and S. I. Seneviratne, 'Development of Future Heatwaves for Different Hazard Thresholds', *Journal of Geophysical Research: Atmospheres*, vol. 125, no. 9, May 2020, doi: 10.1029/2019JD032070.
[13] E. Coffel and R. Horton, 'Climate change and the impact of extreme temperatures on aviation', *Weather, Climate, and Society*, vol. 7, no. 1, pp. 94–102, Jan. 2015, doi: 10.1175/WCAS-D-14-00026.1.
[14] R. Burbidge, 'Adapting aviation to a changing climate: Key priorities for action', *J. Air Transp. Manag.*, vol. 71, pp. 167–174, Aug. 2018, doi: 10.1016/j.jairtraman.2018.04.004.
[15] E. Bucchignani, A. L. Zollo, and M. Montesarchio, 'Analysis of Expected Climate Extreme Variability with Regional Climate Simulations over Napoli Capodichino Airport: A Contribution to a Climate Risk Assessment Framework', *Earth (Switzerland)*, vol. 2, no. 4, pp. 980–996, Dec. 2021, doi: 10.3390/earth2040058.
[16] U. Kale, 'Assessing the impact of climate change on aircraft engine performance during different flight phases (take-off and cruise) and the environmental consequences', *Aircraft Engineering and Aerospace Technology*, vol. 96, no. 7, pp. 912–920, Aug. 2024, doi: 10.1108/AEAT-04-2024-0122.
[17] Z. Hao, F. Hao, V. P. Singh, and X. Zhang, 'Changes in the severity of compound drought and hot extremes over global land areas', *Environmental Research Letters*, vol. 13, no. 12, p. 124022, Dec. 2018, doi: 10.1088/1748-9326/aaee96.
[18] J. Zscheischler *et al.*, 'A typology of compound weather and climate events', *Nat. Rev. Earth Environ.*, vol. 1, no. 7, pp. 333–347, Jun. 2020, doi: 10.1038/s43017-020-0060-z.
[19] C.-H. , S. C. , H. E. , Y. H. , B. S. S. , P. A. , D. A. J. , T. S. O. , F. C. Su, 'BARPA: New development of ACCESS-based regional climate modelling for Australian Climate Service, Bureau Research Report 069', Canberra, 2022. Accessed: Nov. 16, 2025. [Online]. Available: http://www.bom.gov.au/research/publications/researchreports/BRR-069.pdf
[20] Bureau Of Meteorology, 'Bureau of Meteorology Atmospheric Regional Projections for Australia (BARPA) (Version v1.0: 20/12/23)', Canberra, 2023.
[21] E. the E. and W. NSW Department of Climate Change, 'NARCliM2.0 climate projections, NSW Climate Data Portal', Sydney, 2024. Accessed: Nov. 16, 2025. [Online]. Available: https://www.climatechange.environment.nsw.gov.au/climate-data-portal.
[22] C. Tebaldi and R. Knutti, 'The use of the multi-model ensemble in probabilistic climate projections', *Philosophical Transactions of the Royal Society A: Mathematical, Physical and Engineering Sciences*, vol. 365, no. 1857, pp. 2053–2075, Aug. 2007, doi: 10.1098/rsta.2007.2076.
[23] C. Tebaldi *et al.*, 'Climate model projections from the Scenario Model Intercomparison Project (ScenarioMIP) of CMIP6', *Earth System Dynamics*, vol. 12, no. 1, pp. 253–293, Mar. 2021, doi: 10.5194/esd-12-253-2021.
[24] A. Ghaemi, S. A. Hashemi Monfared, A. Bahrpeyma, P. Mahmoudi, and M. Zounemat-Kermani, 'Exploitation of the ensemble-based machine learning strategies to elevate the precision of CORDEX regional simulations in precipitation projection', *Earth Sci. Inform.*, vol. 17, no. 2, pp. 1373–1392, Apr. 2024, doi: 10.1007/s12145-024-01234-5.
[25] J. C. Bennett *et al.*, 'Performance of an empirical bias-correction of a high-resolution climate dataset', *International Journal of Climatology*, vol. 34, no. 7, pp. 2189–2204, Jun. 2014, doi: 10.1002/joc.3830.
[26] H. Zhang, S. Chapman, R. Trancoso, N. Toombs, and J. Syktus, 'Assessing the impact of bias correction approaches on climate extremes and the climate change signal', *Meteorological Applications*, vol. 31, no. 3, May 2024, doi: 10.1002/met.2204.
[27] C. Piani *et al.*, 'Statistical bias correction of global simulated daily precipitation and temperature for the

application of hydrological models', *J. Hydrol. (Amst).*, vol. 395, no. 3–4, pp. 199–215, Dec. 2010, doi: 10.1016/j.jhydrol.2010.10.024.
[28] A. Dosio, P. Paruolo, and R. Rojas, 'Bias correction of the ENSEMBLES high resolution climate change projections for use by impact models: Analysis of the climate change signal', *Journal of Geophysical Research: Atmospheres*, vol. 117, no. D17, Sep. 2012, doi: 10.1029/2012JD017968.
[29] M. Iturbide, A. Casanueva, J. Bedia, S. Herrera, J. Milovac, and J. M. Gutiérrez, 'On the need of bias adjustment for more plausible climate change projections of extreme heat', *Atmospheric Science Letters*, vol. 23, no. 2, Feb. 2022, doi: 10.1002/asl.1072.
[30] Intergovernmental Panel on Climate Change (IPCC), 'Weather and Climate Extreme Events in a Changing Climate', in *Climate Change 2021 – The Physical Science Basis: Working Group I Contribution to the Sixth Assessment Report of the Intergovernmental Panel on Climate Change*, I. P. on C. C. (IPCC), Ed., Cambridge: Cambridge University Press, 2023, pp. 1513–1766. doi: DOI: 10.1017/9781009157896.013.
[31] A. L. Hirsch *et al.*, 'Amplification of Australian Heatwaves via Local Land-Atmosphere Coupling', *Journal of Geophysical Research: Atmospheres*, vol. 124, no. 24, pp. 13625–13647, Dec. 2019, doi: 10.1029/2019JD030665.
[32] I. Mahlstein, C. Spirig, M. A. Liniger, and C. Appenzeller, 'Estimating daily climatologies for climate indices derived from climate model data and observations', *Journal of Geophysical Research: Atmospheres*, vol. 120, no. 7, pp. 2808–2818, Apr. 2015, doi: 10.1002/2014JD022327.
[33] Y. Yosef, E. Aguilar, and P. Alpert, 'Is it possible to fit extreme climate change indices together seamlessly in the era of accelerated warming?', *International Journal of Climatology*, vol. 41, no. S1, Jan. 2021, doi: 10.1002/joc.6740.
[34] C. B. Avcı and M. Vanolya, 'Proposed Framework for Sustainable Flood Risk-Based Design, Construction and Rehabilitation of Culverts and Bridges Under Climate Change', *Water (Basel).*, vol. 17, no. 11, p. 1663, May 2025, doi: 10.3390/w17111663.
[35] V. Gallina, S. Torresan, A. Zabeo, A. Critto, T. Glade, and A. Marcomini, 'A Multi-Risk Methodology for the Assessment of Climate Change Impacts in Coastal Zones', *Sustainability*, vol. 12, no. 9, p. 3697, May 2020, doi: 10.3390/su12093697.
[36] E.-S. Im, N.-X. Thanh, Y.-H. Kim, and J.-B. Ahn, '2018 summer extreme temperatures in South Korea and their intensification under 3 °C global warming', *Environmental Research Letters*, vol. 14, no. 9, p. 094020, Sep. 2019, doi: 10.1088/1748-9326/ab3b8f.
[37] A. T. Michalek, G. Villarini, T. Kim, F. Quintero, W. F. Krajewski, and E. Scoccimarro, 'Evaluation of CMIP6 HighResMIP for Hydrologic Modeling of Annual Maximum Discharge in Iowa', *Water Resour. Res.*, vol. 59, no. 8, Aug. 2023, doi: 10.1029/2022WR034166.
[38] E. D. Coffel, T. R. Thompson, and R. M. Horton, 'The impacts of rising temperatures on aircraft takeoff performance', *Clim. Change*, vol. 144, no. 2, pp. 381–388, Sep. 2017, doi: 10.1007/s10584-017-2018-9.
[39] R. Burbidge, C. Paling, and R. M. Dunk, 'A systematic review of adaption to climate change impacts in the aviation sector', *Transp. Rev.*, vol. 44, no. 1, pp. 8–33, 2023, doi: 10.1080/01441647.2023.2220917.
[40] A. Maslovara and B. Mirković, 'Impact of Tailwind on Airport Capacity and Delay at Zurich Airport', *Transportation Research Procedia*, vol. 59, pp. 117–126, 2021, doi: 10.1016/j.trpro.2021.11.103.
[41] R. Burbidge EUROCONTROL, 'AVOIDING THE PREDICTABLE SURPRISE: EARLY ACTION IS THE KEY TO BUILDING A CLIMATE-RESILIENT AVIATION NETWORK'. [Online]. Available: http://www.eurocontrol.int/articles/challenges-growth.
[42] G. B. Gratton, P. D. Williams, A. Padhra, and S. Rapsomanikis, 'Reviewing the impacts of climate change on air transport operations', *Aeronautical Journal*, vol. 126, no. 1295, pp. 209–221, Jan. 2022, doi: 10.1017/aer.2021.109.
[43] Á. Rodríguez-Sanz, J. Cano, and B. Rubio Fernández, 'Impact of Weather Conditions on Airport Arrival Delay and Throughput', *IOP Conf. Ser. Mater. Sci. Eng.*, vol. 1024, no. 1, p. 012107, Jan. 2021, doi: 10.1088/1757-899X/1024/1/012107.
[44] N. D. Mathasoliya and S. S. Mujumdar, 'Verification of Discharge Carrying Capacity of Existing Stormwater Drain Using New IDF Curves—A Case Study of Vadodara Airport', in *Urbanization Challenges in Emerging Economies*, Reston, VA: American Society of Civil Engineers, Dec. 2018, pp. 691–701. doi: 10.1061/9780784482032.069.
[45] J. Peng, X. Zhong, L. Yu, and Q. Wang, 'Simulating rainfall runoff and assessing low impact development (LID) facilities in sponge airport', *Water Science and Technology*, vol. 82, no. 5, pp. 918–926, Sep. 2020, doi: 10.2166/wst.2020.400.
[46] WMO, 'Aviation Hazards: Convection and Thunderstorms', World Meteorological Organization (https://community.wmo.int/en/activity-areas/aviation/hazards/convection).
[47] R. McGormley, T. Arendt, D. Seal, and E. Fisher, *A Guidebook for Airport Winter Operations*. Washington, D.C.: Transportation Research Board, 2015. doi: 10.17226/22221.